




Transition metal-doped B_n ($n = 7-10$) clusters: confirmation of a circular disk Jellium model

Xue Wu^{1,2}, Yuqing Wang², Xiaoyun Zhao³, Si Zhou^{2,a}, Sidian Li³, Maodu Chen², Jijun Zhao^{2,b} 

¹ State Key Laboratory of Metastable Materials Science and Technology and Key Laboratory for Microstructural Material Physics of Hebei Province, School of Science, Yanshan University, Qinhuangdao 066004, China

² Key Laboratory of Materials Modification by Laser, Ion and Electron Beams (Dalian University of Technology), Ministry of Education, Dalian 116024, China

³ Nanocluster Laboratory, Institute of Molecular Science, Shanxi University, Taiyuan 030006, China

Received: 10 September 2020 / Accepted: 13 March 2021

© The Author(s), under exclusive licence to Società Italiana di Fisica and Springer-Verlag GmbH Germany, part of Springer Nature 2021

Abstract Using a genetic algorithm combined with density functional theory calculations, we have performed a systematic global search for the low-lying structures of $4d$ and $5d$ transition metal (M)-doped B_n clusters with $n = 7-10$. Diverse structural patterns have been identified as the ground state for MB_n clusters, i.e., half-sandwich for early transition metal dopants, wheel-like configuration for middle transition metal dopants, quasi-planar and umbrella-like structures for late transition metal dopants. Among them, the half-sandwich RhB_7 , IrB_7 , RuB_8 and OsB_8 ; wheel-like IrB_9 ; and umbrella-like AgB_9 and AuB_9 clusters have relatively high stability, which are not only stabilized by the closed-shell occupation following a circular disk Jellium model, but also enhanced by aromaticity with the π bonds distributed over the circular disk. Our results not only enrich the family of 2D superatomic clusters but also advance the fundamental understanding of the metal-doped boron clusters.

1 Introduction

Boron and its compounds have attracted considerable interests owing to their unusual chemical bonding and novel chemical/physical properties [1–6]. With unique nature of electron deficiency, B atom can bond with most elements via a favorable delocalized multicenter bond. To date, many experimental and computational investigations revealed the diverse structural patterns of pure B_n clusters, such as planar, quasi-planar, bilayer, tubular, cage-like and core-shell structures [6–10].

The small-sized B_n clusters ($n < 20$) are dominated by planar or quasi-planar configurations, which are stabilized by electron delocalization in both σ and π frameworks. Among

Electronic supplementary material The online version contains supplementary material available at <https://doi.org/10.1140/epjp/s13360-021-01315-0>.

^a e-mail: sizhou@dlut.edu.cn (corresponding author)

^b e-mail: zhaojj@dlut.edu.cn (corresponding author)

them, highly symmetrical wheel-like B_7^- , B_8^- and B_9^- are distinctively characterized by the presence of a central B atom [11, 12], which further motivate systematic explorations on substitutional doping of the central B atom [13–18]. Ito et al. predicted several planar hypercoordinate CoB_8^- , FeB_9^- and FeB_8^{2-} clusters, which are stabilized by “double aromatic” character with six π electrons and ten radical electrons [19, 20]. These cluster species were later confirmed by the experimental photoelectron spectroscopic studies by Wang and coworkers [16, 17]. Wang’s group also proposed an electronic design principle based on the double aromaticity requirement to achieve stable transition metal-centered planar B_n clusters [16]. Following this principle, many clusters have been obtained, such as $RuB_9^{0/-}$, $RhB_9^{0/-}$, $IrB_9^{0/-}$, Re_9^- , TaB_{10}^- , NbB_{10}^- , etc. [21–23]. So far, the planar metal-centered B_n clusters with highest coordination number are TaB_{10}^- and NbB_{10}^- [22]. Considering the proper atomic sizes and number of valence electrons, the transition metal (M) elements with partially filled d orbitals are more suitable as the central dopant to stabilize a B_n wheel by forming delocalized bonds with B atoms.

In addition to the metal-centered wheel-like structures, several other structural motifs were also identified in small-size metal-doped B_n clusters. A typical one is the half-sandwich structure, which is a bipyramid with a metal atom located at the apical site. Liu et al. [24] investigated $3d$ transition metal-doped B_n clusters and found $n = 7$ marks the onset of the half-sandwich structure, among which CrB_7 , FeB_7 and CoB_7 clusters possess relatively higher stabilities. Later, AlB_7 , AlB_8 and PrB_7 were featured as a metal atom interacting ionically with a hexagonal B_7 (C_{6v}) or heptagonal B_8 (C_{7v}) pyramidal fragment [14, 25]. As the B_7^{3-} and B_8^{2-} molecular wheels satisfy double aromaticity, ligands bonding with a metal dopant further enhance their stability. When $n < 7$, the metal dopant prefers staying at the edges of B_n clusters [24, 26, 27]. For instance, MB_6 favors a hexagonal geometry with a B atom in the center and the metal atom located at the edge site [28, 29]. For $n \geq 10$, most metal-doped B_n clusters adopt bowl-like or drum-shaped structures [30–33].

Despite many reports on the metal-doped boron clusters, little is known about the small-size B_n clusters doped with a late transition metal atom. Besides the distinctive wheel-like and half-sandwich structures, are there any other structural patterns in this size range? What is the bonding character between the d orbitals of the transition metal atom and the $2s$ and $2p$ orbitals of B atoms? In this work, we present a systematic study on $4d$ and $5d$ transition metal-doped boron clusters in order to elucidate the structural patterns and bonding characters of MB_n ($n = 7–10$). In addition to the known wheel-like and half-sandwich structural patterns, an umbrella-like structure is found in AgB_9 and AuB_9 for the first time. Among all the considered clusters, the half-sandwich RhB_7 , IrB_7 , RuB_8 and OsB_8 and umbrella-like AgB_9 and AuB_9 clusters exhibit higher stability, which can be correlated to their closed electron shells following a Jellium model of the circular disk.

2 Methods

Unbiased global search of MB_n ($n = 7–10$) clusters was carried out using our own comprehensive genetic algorithm (CGA) code [34] incorporated with density functional theory (DFT) calculations [35] (CGA-DFT). For each cluster, CGA search was conducted with at least 1000 iterations for a population of 12 members to ensure the global minimum structure within the used computational approach. The child clusters from crossover and optional mutation operations were fully relaxed using the double numerical basis set plus d -polarization functions (DND) combined with the Perdew–Burke–Enzerhof (PBE) functional within the generalized gradient approximation (GGA) [36, 37], as implemented in the DMol³ program

[35]. The validity and efficiency of the present CGA-DFT scheme have been well demonstrated in our recent studies on B [10, 38] and doped B [39, 40] clusters. Further details of CGA can be found in the review articles [34, 41].

The low-lying isomers from CGA-DFT search were further optimized by considering different spin multiplicities at higher accuracy, with the PBE0 functional [42], and 6-311 + G(d) and LANL2DZ basis sets for B and M atoms, respectively. To confirm the PBE0 results, the relative energies between some selected isomers were further calculated at the CCSD(T) level with the same basis sets [43]. By computing the vibrational frequencies of these MB_n clusters, we verified that there is no imaginary frequency corresponding to the saddle point on the potential energy surface, and we added the zero-point-energy (ZPE) to the total energy of each isomer. The energetic stability of a MB_n cluster is characterized by the doping energy (E_d) of M atom defined as:

$$E_d(MB_n) = E(B_n) + E(M) - E(MB_n), \quad (1)$$

where $E(MB_n)$ is energy of the MB_n cluster, $E(B_n)$ is the energy of the B_n moiety in MB_n without structural relaxation, and $E(M)$ is the energy of an individual M atom, respectively. Chemical bonding analyses were performed using the natural bond orbital (NBO) and adaptive natural density partitioning (AdNDP) methods [44, 45]. The nucleus-independent chemical shift (NICS) [46] and zz NICS shielding tensor components (NICS_{zz}) [47] were computed to assess the aromaticity. Except for CGA-DFT search, all of the above calculations and analyses were performed using the Gaussian 09 package [48].

3 Results and discussion

3.1 Global minimum structures of MB_n clusters

The ground-state structures of MB_n clusters ($n = 7-10$) from our high-throughput structural searches are presented in Fig. 1 and Fig. S1–S4 of Supporting Information. All these 72 cluster structures can be classified into half-sandwich, wheel-like, umbrella-like, and quasi-planar structural patterns. Among them, the umbrella-like one has never been reported before.

For $4d$ transition metals, the MB_n clusters doped with early and middle M elements adopt half-sandwich structures with the quasi-planar B_7 (C_{6v}), B_8 (C_{7v}), B_9 (C_s) and B_{10} (C_{2v}) moieties coordinated to the M atom, while the late M-doped B_n clusters usually prefer quasi-planar B_n configuration with the M atom located at the low-coordination peripheral position. As exceptional cases, the lowest energy structures of RhB_9 and PdB_9 are formed by an RhB_2 trimer and a PdB dimer bonded with quasi-planar B_7 and B_8 moieties, respectively. Interestingly, the ground state of AgB_9 is an unprecedented umbrella-like structure with C_{7v} symmetry. It is constructed by an $Ag-B$ heteronuclear dimer bonded with the B_8 unit (C_{7v}), with the closed d -shell Ag atom having low coordination.

Similar to the cases of $4d$ transition metal doping, the $5d$ transition metal-doped B_n clusters adopt hypercoordinated half-sandwich or wheel-like structures for early and middle M atoms and lower-coordinated quasi-planar or umbrella-like structures for late M atoms, respectively. Roughly speaking, the half-sandwich pattern dominates the ground states for most considered MB_n clusters. The M dopant atoms prefer the high-coordinated center of half-sandwich, except TaB7 having the Ta atom replacing a B atom on the peripheral ring of B_7 framework. As the cluster size increases, the first wheel-like structure occurs at the critical size $n = 8$, among which the quartet spin state of ReB_8 agrees with the previous report by Chen et al. [23] and the doublet spin state of IrB_8 is found for the first time.

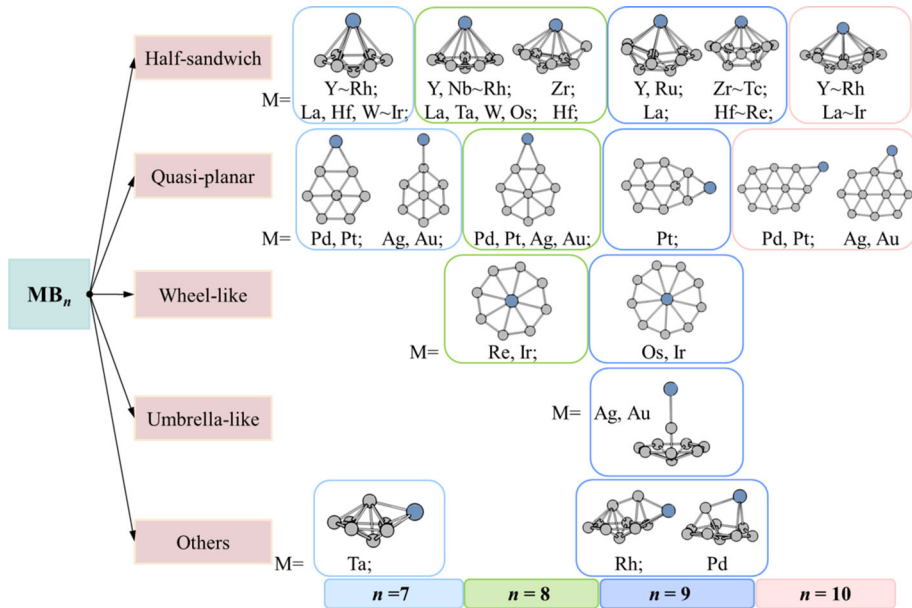


Fig. 1 Structural patterns of MB_n ($n = 7-10$) clusters. The tilde symbol (\sim) between Y and Rh, W and Ir, Nb and Rh means that the elements belonging to the same period of the periodic table between those two elements (e.g., $Y \sim Rh$ means Y, Zr, Nb, Mo, Tc, Ru, Rh)

Noticeably, a half-sandwich OsB_8 cluster with singlet electronic state emerges between the wheel-like structural pattern (ReB_8 and IrB_8). Thus, not only the cluster size but also the specific electronic configuration play more important roles in determining the ground-state structure of M-centered B_n clusters.

Among the considered MB_n clusters, the highest coordination number in the wheel-like species is nona-coordinated OsB_9 and IrB_9 clusters with C_{9v} symmetry. IrB_9 has a singlet spin multiplicity and has been reported by Li et al. [21], while OsB_9 with doublet spin state is reported for the first time. However, the wheel-like ReB_9 structure suggested by Chen et al. [23] is higher in energy by 0.39 eV than the half-sandwich one according to our PBE0 calculation. Generally speaking, $5d$ M atoms are suitable central dopants in the eight- and nine-membered rings of boron, such as the cases of ReB_8 , IrB_8 , OsB_9 and IrB_9 , while the isoelectronic $4d$ M atoms are too small to stabilize the B_8 and B_9 wheels. The umbrella-like pattern only occurs for MB_9 clusters doped with the group IB elements, i.e., AgB_9 and AuB_9 .

With increasing number of B atoms, the growth behavior of MB_n clusters can be viewed as gradually adding B atom on the quasi-planar skeleton of B_n . Some exceptional cases are wheel-like and umbrella-like patterns in the middle or late transition metal-doped B_n clusters, respectively. Up to $n = 10$, the preferred structural pattern becomes relatively simpler, i.e., either C_{2v} half-sandwich or C_1 quasi-planar structure. The B_{10} ligand framework is a fragment of triangular lattice similar to the bare B_{10} cluster, in which two interior B atoms are surrounded by eight peripheral B atoms [49].

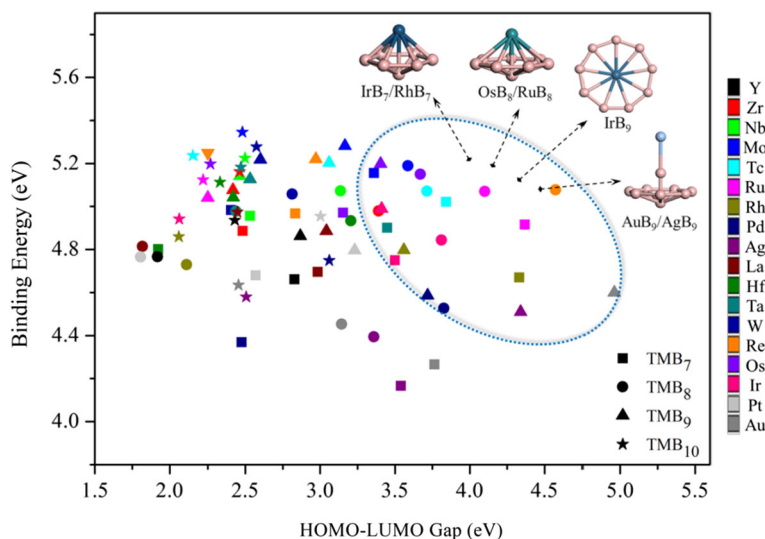


Fig. 2 Scatter plots of relative stability of MB_n ($n = 7-10$) clusters. Shapes and colors of the data points indicate the cluster sizes n and type of M elements, respectively. The clusters with higher binding energy (E_b), larger HOMO–LUMO gap (E_{HL}) and higher symmetry are enclosed by the dotted circles, and the structures of clusters with closed electronic shell are shown as insets

3.2 Stabilities of MB_n clusters

To discuss the relative stability of MB_n ($n = 7-10$) clusters, the average binding energy (E_b) and HOMO–LUMO gap (E_{HL}) are plotted in Fig. 2 for all the 72 clusters. Intuitively, those clusters occupying the upper right region (highlighted by the dotted circle in Fig. 2) possess relatively higher thermodynamic and chemical stabilities. Among them, the half-sandwich RhB_7 , IrB_7 , RuB_8 and OsB_8 ; wheel-like IrB_9 ; and umbrella-like AgB_9 and AuB_9 clusters stand out with large HOMO–LUMO gap ($E_{HL} > 3.4$ eV) and appreciable binding energy ($E_b > 4.5$ eV) owing to their closed electronic shell. Our CCSD(T) calculations further confirm that these MB_n cluster structures are indeed the ground states (see Table S1). To further support the results about the first reported umbrella-like AgB_9 and AuB_9 clusters, we examined the adiabatic electron affinity (AEA) and the relative energies of low-lying isomers of them using a variety of common functionals including HSE06, B3LYP, B3PW91 and TPSSh. The umbrella-like AgB_9-I and AuB_9-I with the smallest AEA are always the ground-state structures calculated with different functionals (see Table S2). In the following contents, we will focus on these seven relatively stable clusters.

Furthermore, the energetic stability of the above clusters can be characterized by the doping energy (E_d) of M atom defined in Eq. (1). As shown in Table 1, the clusters with higher coordination have larger doping energy. For instance, IrB_9 cluster with nona-coordination on Ir has a giant E_d of 13.18 eV, while AgB_9 cluster with lower coordination of M atom has an E_d of only 2.41 eV. Moreover, the doping energy of the $4d$ -M-doped cluster is slightly larger than the isoelectronic $5d$ -M-doped cluster within the same half-sandwich pattern. In addition, the total Wiberg bond indexes (WBI) of the M atom (WBI_M) range from 0.86 (AgB_9) to 4.42 (OsB_8), and the total WBI of $5d$ -M is larger than that of $4d$ -M in the same structural pattern. All these results imply that the $5d$ -M atom has stronger interaction with the B_n moiety than that of $4d$ -M. Meanwhile, the average WBI of M–B(peripheral) (i.e., WBI_{M-B1}) is larger

Table 1 Binding energy per atom (E_b), HOMO–LUMO gap (E_{HL}), doping energy (E_d), and Wiberg bond indexes (WBI_M , WBI_{M-B1} and WBI_{M-B2}) of M total bond order, average M–B(peripheral) bond and M–B(central) bond of MB_n clusters

Cluster	E_b (eV)	E_{HL} (eV)	E_d (eV)	WBI_M	WBI_{M-B1}	WBI_{M-B2}
RhB ₇	4.67	4.33	6.55	2.92	0.45	0.20
IrB ₇	4.75	3.50	7.35	3.52	0.53	0.32
RuB ₈	5.07	4.10	9.63	3.81	0.49	0.37
OsB ₈	5.15	3.67	10.46	4.42	0.56	0.50
IrB ₉	4.99	3.41	13.18	4.37	0.49	–
AgB ₉	4.51	4.34	2.41	0.86	–	0.67
AuB ₉	4.60	4.96	3.38	1.17	–	0.96

than that of M–B(central) (i.e., WBI_{M-B2}), suggesting that the M atom bonds stronger with peripheral B atoms than with central B atom in the half-sandwich pattern. Among them, the OsB₈ cluster has the largest WBI_M and WBI_{M-B1} values, associated with the largest binding energy of 5.15 eV. In the umbrella-like AgB₉ and AuB₉ clusters, the WBI_{M-B2} values are 0.67 and 0.96, respectively, reflecting appreciable interactions between the M atom and the adjacent B atoms.

For a cluster or molecule, the vertical ionization potential (VIP) and vertical electron affinity (VEA) are characteristic electronic properties that describe the capability to loss or gain an electron, while the difference between VIP and VEA known as the chemical hardness [50, 51] is a useful metric for estimating the stability of the cluster. In addition, the adiabatic electron affinity (AEA) is also calculated to evaluate the chemical stability of cluster, which is defined as the binding energy of an electron to the neutral cluster. All these values for the seven highly stable MB_n ($n = 7–10$) clusters are summarized in Table 2. The chemical hardness for these clusters are relatively large, i.e., ranging from 6.51 eV (IrB₇) to 8.07 eV (AuB₉), much larger than those of other MB_n clusters with singlet state (i.e., 5.43 eV and 6.03 eV for half-sandwich YB₇ and LaB₇, 6.52 eV and 4.92 eV for quasi-planar AgB₇ and PtB₈, respectively, shown in Table S3). Meanwhile, these values are larger than that of the typical 2D closed-shell cluster like Au₆ (6.52 eV) and comparable to those of the larger-size metal-capsulated boron cages W@B₂₄ and Mo@B₂₄ with 18-electron closed shell (7.13 and 6.81 eV). Moreover, the differences of VIP and VEA of 5d-M dopants are larger than those of 4d-M dopants within the same structural pattern implying that the 5d-M-doped B_n clusters with larger chemical hardness would possess higher stability. The relatively small AEA values mean high stability of those closed-shell clusters and are consistent with their large HOMO–LUMO gap. In addition, NBO analyses unveil that the M atom in the wheel-like pattern possesses negative charge and thus acts as an electron acceptor, while it holds positive charge in umbrella-like pattern and generally remains electric neutrality in the half-sandwich pattern.

Compared to the umbrella-like AgB₉ (AuB₉) cluster, the quasi-planar C_s AgB₈ and C₁ AgB₁₀ (AuB₈ and AuB₁₀) with an Ag (Au) atom bound at the edge show relatively low stability. Intuitively, this is because the quasi-planar ones have lower symmetry. Meanwhile, with open electronic configuration, the quasi-planar ones have smaller HOMO–LUMO gap and larger AEA, and the chemical hardness for these clusters are relatively weak (see Table S4), i.e., ranging from 4.79 eV (AuB₁₀) to 5.46 eV (AgB₈), much smaller than 7.38 eV (AgB₉) and 8.07 eV (AuB₉). Furthermore, the AdNDP analyses reveal a single electron

Table 2 Vertical ionization potentials (VIP), vertical electron affinities (VEA), adiabatic electron affinities (AEA), difference between VIP and VEA, and natural population analysis (NPA) charges of M atoms, and NICS_{zz} values corresponding to NICS(0)_{zz} at the geometry center (NICS(1)_{zz} at a point 1.0 Å above the ring center for IrB₉ only)

Cluster	VIP (eV)	VEA (eV)	AEA (eV)	VIP–VEA (eV)	NPA (e)	NICS _{zz} (ppm)
RhB ₇	8.51	1.13	1.33	7.38	0.09	– 81.8
IrB ₇	8.36	1.85	1.92	6.51	0.17	– 83.4
RuB ₈	8.36	1.43	1.57	6.94	– 0.06	– 105.3
OsB ₈	8.28	1.77	1.82	6.51	0.04	– 104.8
IrB ₉	8.86	2.49	2.55	6.37	– 0.38	– 75.0
AgB ₉	8.39	1.01	1.15	7.38	0.55	– 61.4
AuB ₉	9.12	1.05	1.44	8.07	0.31	– 52.9

occupying one π bond in AgB₈ (AuB₈) cluster, which deviates from the $4N + 2$ Hückel rule of aromaticity (see Fig. S5 a–d). The detailed information about the bonding nature will be discussed in Sect. 3.3.

3.3 Chemical bond analysis

Based on the analyses of relative stability, we further choose half-sandwich IrB₇ and RuB₈, wheel-like IrB₉ and umbrella-like AgB₉ clusters as examples to probe the bonding nature between the M atom and the B_n moiety by AdNDP analyses (Fig. 3). The clusters with identical structural pattern are shown in Fig. S6.

For the half-sandwich IrB₇ and RuB₈ clusters, the AdNDP analyses [52, 53] reveal 2c–2e σ bonds on the B–B bond of circumference, including six σ bonds for IrB₇ and seven σ bonds for RuB₈, three lone pairs on the Ir and Ru atom, and six completely delocalized σ and π bonds for both clusters. The AdNDP analysis of the umbrella-like AgB₉ cluster gives more complicated bonding characters, that is, an extra 2c–2e σ bond located on Ag–B besides the seven 2c–2e σ bonds on the B–B bonds of circumference. Moreover, five lone pairs on the Ag atom and six delocalized 9c–2e σ and π bonds on the B₉ ligand are revealed. The wheel-like IrB₉ has nine 2c–2e σ B–B bonds, three lone pairs on the Ir atom, and six completely delocalized σ and π bonds, obeying the $4N + 2$ Hückel rule of aromaticity and consistent with the results by Li et al. [21] In addition, the AdNDP analyses reveal that the clusters with high spin state have similar chemical bonding characteristic with the closed-shell ones in the same structural patterns. In other words, the chemical bonding characteristic is closely related to the structural pattern, while the spin state of cluster may only affect the specific occupations of some bonding orbitals by single or dual electrons (see Fig. S5 e–f).

The NICS(0)_{zz} at the geometry center of half-sandwich clusters in the range of – 81.8 to – 105.3 ppm (Table 2) suggest their very strong aromatic character. The umbrella-like AgB₉ and AuB₉ clusters also have considerable NICS(0)_{zz} values (– 61.4 and – 52.9 ppm). The NICS_{zz} at a point 1.0 Å above the ring center (NICS(1)_{zz}) of wheel-like IrB₉ cluster is – 75.9 ppm, which is much larger than benzene (– 10.3 ppm) and corresponds to the doubly aromaticity. These values are comparable to the NICS(1)_{zz} values of wheel-like CoB₉ cluster (– 85.4 ppm) reported by Ito et al. [19] In other words, aromaticity or doubly aromaticity plays an essential role in the stability of these MB_n clusters.

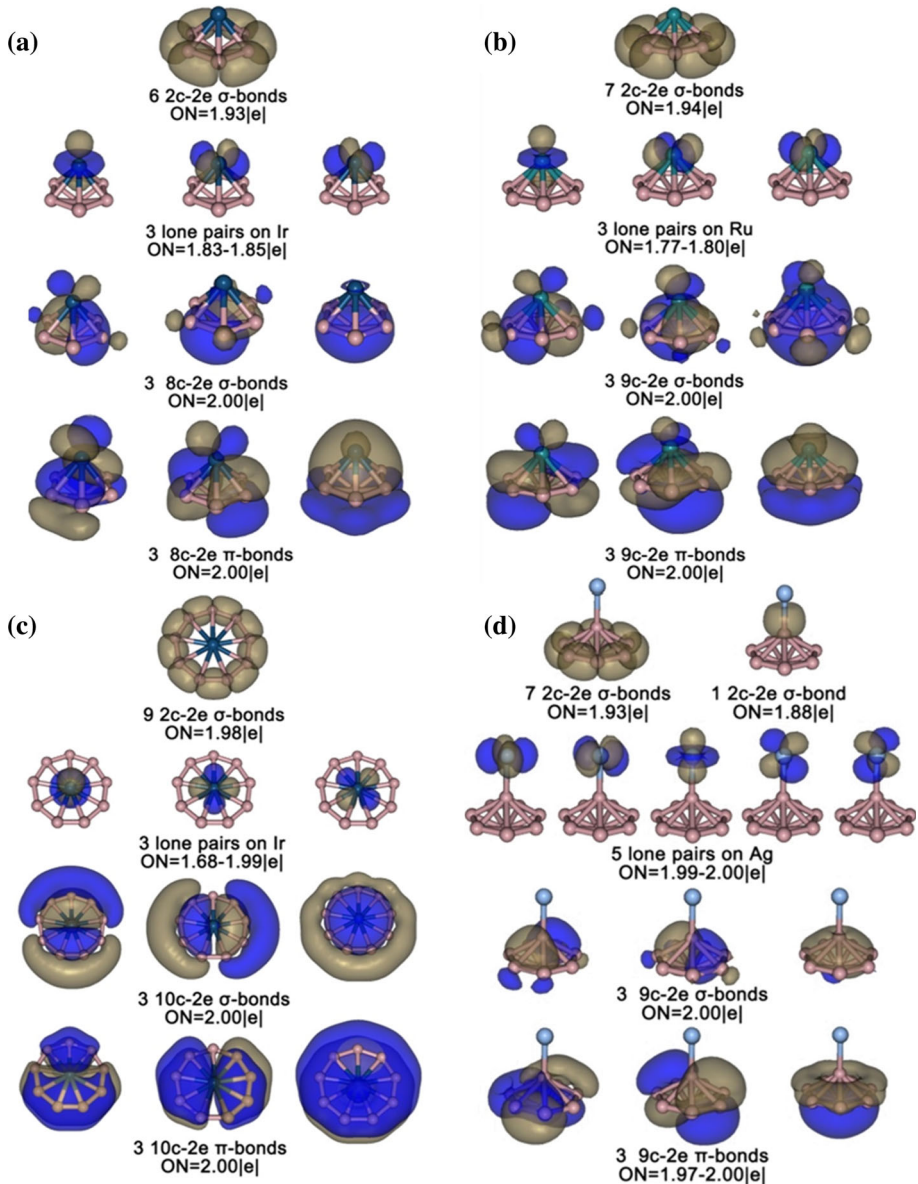


Fig. 3 AdNDP chemical bonding patterns of **a** IrB₇, **b** RuB₈, **c** IrB₉, and **d** AgB₉ clusters with the occupation number (ON)

3.4 Two-dimensional superatomic clusters

From the above discussions, all these relatively stable clusters adopt nearly circular disk geometries with completely delocalized π system obeying the $4N + 2$ Hückel rule of aromaticity. Intuitively, it is tempting to ascribe the enhanced stability of these MB_{*n*} clusters to the closed electron shell in a disk jellium model [54, 55], which has been success-

fully applied to pure and transition metal-doped Au clusters as well as P- or Si-doped B_n clusters [56–59]. In the case of circular clusters with superatomic orbital in sequence of $1S^2 1P^4 1D^4 2S^2 1F^4 2P^4 1G^4 2D^4 3S^2 \dots$, enhanced stabilities are expected to occur at 2, 6, 10, 12, 16, 20, 24, 28, 30... valence electrons, which are in fact related to the concept of “aromaticity” [60]. For instance, the aromaticity of a benzene molecule arises from six delocalized p electrons forming a delocalized π system in a hexagonal confinement, and the electronic configuration is thus analogous to $1S^2 1P^4$.

The energy levels and spatial distributions of the occupied molecular orbitals of these relatively stable clusters (e.g., IrB_7 , RuB_8 , IrB_9 and AgB_9) are illustrated in Fig. 4. Obviously, all of them behave as 2D superatoms with orbitals that can be categorized into 2D superatomic molecular orbitals. Interestingly, three orbitals (with possible degeneracy) in each cluster are recognized as π bonds, which are consistent with the delocalized π -bonding based on the AdNDP analyses. For example, HOMO–4 and HOMO–6 of IrB_7 , HOMO–3 and HOMO–6 of RuB_8 , HOMO–2 and HOMO–5 of IrB_9 as well as HOMO–2 and HOMO–9 of AgB_9 cluster. Those π bonds are perpendicular to the circular disk and distributed over the upper and lower surfaces, which play an important role in the structural stability of circular disk. The valence electrons distributed in-plane are participating in the 2D superatomic orbitals except the lone pairs on M atom.

After subtracting the six π -bonding electrons, the half-sandwich IrB_7 and RuB_8 clusters have 24 and 26 remaining valence electrons, respectively, forming a closed electronic shell $1S^2 1P^4 1D^4 2S^2 1F^4 (1F^2) 2P^4 2D^4 3S^2$ configuration. The wheel-like IrB_9 cluster has 30 remaining valence electrons: 2 electrons (d_{z^2} lone pair) being localized on the Ir atom (HOMO–1) and the rest 28 electrons forming a closed electronic shell $1S^2 1P^4 1D^4 1F^4 2S^2 1G^4 2D^4 2P^4$ configuration. The umbrella-like AgB_9 has 32 remaining valence electrons: 5 lone pairs on the Ag atom (HOMO–4, HOMO–6, HOMO–7), one σ bond on Ag–B (HOMO) and the rest 20 electrons forming a closed electronic shell $1S^2 1P^4 1D^4 2S^2 1F^4 2P^4$ configuration.

4 Conclusions

A systematic investigation on the structural and electronic properties of $4d$ and $5d$ M-doped B_n ($n = 7–10$) clusters has been performed using the comprehensive genetic algorithm structural searches combined with DFT calculations. For both $4d$ and $5d$ transition metal elements, MB_n clusters adopt hypercoordinated half-sandwich for early M dopants, wheel-like structures for middle M dopants and lower-coordinated quasi-planar or umbrella-like structures for late M dopants. Strikingly, the half-sandwich RhB_7 , IrB_7 , RuB_8 and OsB_8 ; wheel-like IrB_9 ; and umbrella-like AgB_9 and AuB_9 clusters exhibit high stability, which carry “magic number” valence electrons occupying the closed electronic shells and following a disk jellium model. Chemical bonding analysis reveals that the rest delocalized π bonds distributed over the circular disk play a key role in their structural stability. These theoretical results establish a complete picture of the $4d$ and $5d$ M-doped boron clusters, which have high symmetry and appreciable stability. The present study may promote experimental synthesis of these intriguing B-based 2D superatom clusters as building block of nanomaterials.

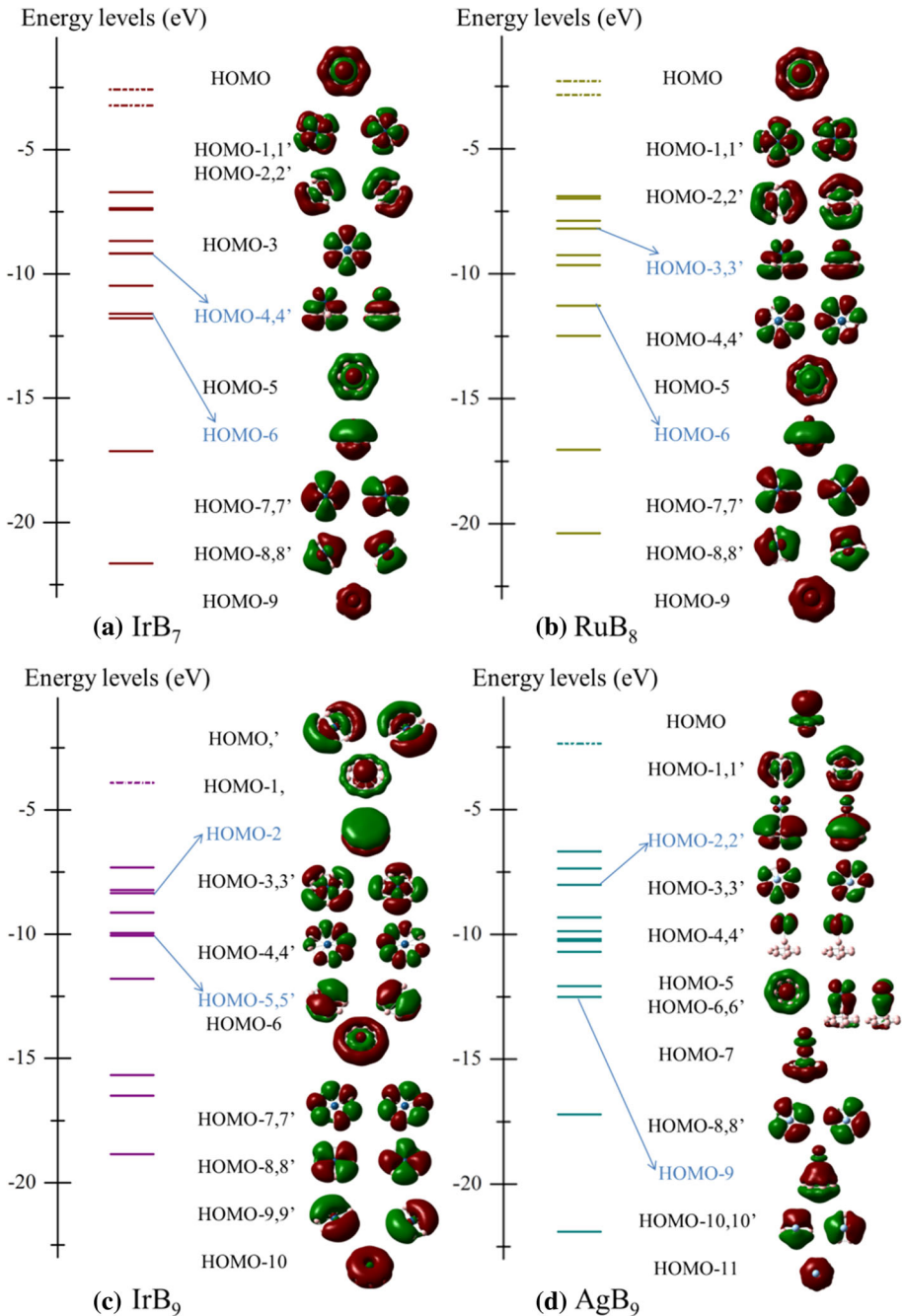


Fig. 4 Energy levels and corresponding molecule orbitals of IrB₇, RuB₈, IrB₉ and AgB₉ clusters. The unoccupied orbitals are indicated in dotted line. The arrows indicate the π bonding orbitals

Acknowledgements This work was supported by the National Natural Science Foundation of China (91961204, 11804076, 11974068 and 11904251), the Fundamental Research Funds for the Central Universities of China (DUT20LAB110) and the Supercomputing Center of Dalian University of Technology. We thank Prof. Vijay Kumar in Shiv Nadar University for stimulating discussions.

References

1. C. Romanescu, T.R. Galeev, W.L. Li, A.I. Boldyrev, L.S. Wang, *Acc. Chem. Res.* **46**(2), 350 (2013)
2. L.M. Yang, E. Ganz, Z. Chen, Z.X. Wang, P.V.R. Schleyer, *Angew. Chem. Int. Ed.* **54**(33), 9468 (2015)
3. B.P.T. Fokwa, M. Hermus, *Angew. Chem. Int. Ed.* **51**, 1702 (2012)
4. Q. Zheng, M. Kohout, R. Gumenuik, N. Abramchuk, H. Borrmann, Y. Prots, U. Burkhardt, W. Schnelle, L. Akselrud, H. Gu, A. Leithe-Jasper, Y. Grin, *Inorg. Chem.* **51**(14), 7472 (2012)
5. J.J. Zhao, Q.Y. Du, S. Zhou, V. Kumar, *Chem. Rev.* **120**, 9021 (2020)
6. W.L. Li, X. Chen, T. Jian, T.T. Chen, J. Li, L.S. Wang, *Nat Rev Chem* **1**, 0071 (2017)
7. I. Boustani, *Phys. Rev. B* **55**(24), 16426 (1997)
8. A.N. Alexandrova, A.I. Boldyrev, H.J. Zhai, L.-S. Wang, *Coord. Chem. Rev.* **250**, 2811 (2006)
9. L.-S. Wang, *Int. Rev. Phys. Chem.* **35**(1), 69 (2016)
10. X. Wu, L. Sai, S. Zhou, P. Zhou, M. Chen, M. Springborg, J. Zhao, *Phys. Chem. Chem. Phys.* **22**, 12959 (2020)
11. H.J. Zhai, A.N. Alexandrova, K.A. Birch, A.I. Boldyrev, L.S. Wang, *Angew. Chem. Int. Ed.* **42**, 6004 (2003)
12. D.Y. Zubarev, A. I. Boldyrev, *J. Comput. Chem.* **28**(1), 251 (2007)
13. Z. Yang, S. J. Xiong, *J. Chem. Phys.* **128**(18), 184310 (2008)
14. T.R. Galeev, C. Romanescu, W.L. Li, L.S. Wang, A.I. Boldyrev, *J. Chem. Phys.* **135**(10), 104301 (2011)
15. W.L. Li, C. Romanescu, T.R. Galeev, L.S. Wang, A.I. Boldyrev, *J. Phys. Chem. A* **115**(38), 10391 (2011)
16. C. Romanescu, T.R. Galeev, W.L. Li, A.I. Boldyrev, L.S. Wang, *Angew. Chem. Int. Ed.* **50**(40), 9334 (2011)
17. C. Romanescu, T.R. Galeev, A.P. Sergeeva, W.L. Li, L.S. Wang, A.I. Boldyrev, *J. Organomet. Chem.* **721–722**, 148 (2012)
18. A.C. Reber, S. N. Khanna, *J. Chem. Phys.* **142**(5), 054304 (2015)
19. K. Ito, Z. Pu, Q.S. Li, P.V.R. Schleyer, *Inorg. Chem.* **47**(23), 10906 (2008)
20. Z. Pu, K. Ito, P.V.R. Schleyer, Q.S. Li, *Inorg. Chem.* **48**(22), 10679 (2009)
21. W.L. Li, C. Romanescu, R. Timur, Z.A. Piazza, A.I. Boldyrev, L.S. Wang, *J. Am. Chem. Soc.* **134**(1), 165 (2012)
22. T.R. Galeev, C. Romanescu, W.L. Li, L.S. Wang, A.I. Boldyrev, *Angew. Chem. Int. Ed.* **51**(9), 2101 (2012)
23. T.T. Chen, W.L. Li, H. Bai, W.J. Chen, X.R. Dong, J. Li, L.S. Wang, *J. Phys. Chem. A* **123**(25), 5317 (2019)
24. X. Liu, G.-F. Zhao, L.-J. Guo, Q. Jing, Y.-H. Luo, *Phys. Rev. A* **75**, 063201 (2007)
25. T.T. Chen, W.L. Li, J. Tian, C. Xin, J. Li, L.S. Wang, *Angew. Chem. Int. Ed.* **56**(24), 6916 (2017)
26. P. Li, T. Mei, L. Lv, C. Lu, W. Wang, G. Bao, G.L. Gutsev, *J. Phys. Chem. A* **121**(34), 6510 (2017)
27. P. Li, G. Sun, J. Bai, W. Wang, G. Bao, C. Lu, *New J. Chem.* **41**, 11208 (2017)
28. L.F. Cheung, J. Czekner, G.S. Kocheril, L.-S. Wang, *J. Am. Chem. Soc.* **2019**(141), 17854 (2019)
29. L.F. Cheung, G.S. Kocheril, J. Czekner, L.-S. Wang, *J. Phys. Chem. A* **2020**(124), 2820 (2020)
30. B. Chen, W. Sun, X. Kuang, C. Lu, X. Xia, H. Shi, G.L. Gutsev, *Phys. Chem. Chem. Phys.* **20**(48), 30376 (2018)
31. B.L. Chen, W.G. Sun, X.Y. Kuang, C. Lu, X.X. Xia, H.X. Shi, G. Maroulis, *Inorg. Chem.* **57**, 343 (2018)
32. W.L. Li, C. Romanescu, Z.A. Piazza, L.S. Wang, *Phys. Chem. Chem. Phys.* **14**(39), 13663 (2012)
33. I.A. Popov, W.-L. Li, Z.A. Piazza, A.I. Boldyrev, L.S. Wang, *J. Phys. Chem. A* **118**, 8098 (2014)
34. J. Zhao, R. Shi, L. Sai, X. Huang, Y. Su, *Mol. Simulat.* **42**(10), 809 (2016)
35. B.J. Delley, *J. Chem. Phys.* **113**(18), 7756 (2000)
36. J.P. Perdew, K. Burke, M. Ernzerhof, *Phys. Rev. Lett.* **78**(7), 1396 (1997)
37. J.P. Perdew, K. Burke, M. Ernzerhof, *Phys. Rev. Lett.* **77**(7), 3865 (1996)
38. L. Sai, X. Wu, N. Gao, J. Zhao, R.B. King, *Nanoscale* **9**, 13905 (2017)
39. Y. Wang, X. Wu, J. Zhao, *J. Clust. Sci.* **29**(5), 847 (2018)
40. X. Wu, S.J. Lu, X. Liang, X. Huang, Y. Qiu, M. Chen, J. Zhao, H.G. Xu, R.B. King, W. Zheng, *J. Chem. Phys.* **146**(4), 044306 (2017)
41. S. Zhou, Y. Zhao, J. Zhao, *Chin. J. Struct. Chem.* **39**, 1185 (2020)

42. C. Adamo, V. Barone, *J. Chem. Phys.* **110**(13), 6158 (1999)
43. G.D. Purvis, J. Bartlett, *J. Chem. Phys.* **76**(4), 1910 (1982)
44. D.Y. Zubarev, I. Boldyrev, *Phys. Chem. Chem. Phys.* **10**(34), 5207 (2008)
45. T. Lu, F. Chen, *J. Comput. Chem.* **33**(5), 580 (2012)
46. Z. Chen, B. King, *Chem. Rev.* **105**(10), 3613 (2005)
47. E. Steiner, P.W. Fowler, L.W. Jenneskens, *Angew. Chem. Int. Ed. Engl.* **40**(2), 362 (2001)
48. M.J. Frisch, G.W. Trucks, H.B. Schlegel, G.E. Scuseria, M. Robb, J.R. Cheeseman, G. Scalmani, V. Barone, B. Mennucci, G.A. Petersson, (Gaussian Inc, Wallingford, 2009)
49. H.J. Zhai, B. Kiran, J. Li, L.S. Wang, *Nat. Mater.* **2**(12), 827 (2003)
50. R.G. Parr, G. Pearson, *J. Am. Chem. Soc.* **105**(26), 7512 (1983)
51. R.G. Pearson, *J. Chem. Sci.* **117**(5), 369 (2005)
52. W.Z. Yao, J.B. Yao, X.B. Li, S.D. Li, *Acta Phys. Chim. Sin.* **29**(6), 1219 (2013)
53. W.Z. Yao, Z.H. Lu, S.D. Li, *Acta Phys. Chim. Sin.* **30**(12), 2233 (2014)
54. S.M. Reimann, M. Koskinen, H. Hakkinen, P.E. Lindelof, M. Manninen, *Phys. Rev. B* **56**(19), 12147 (1997)
55. S.M. Reimann, M. Koskinen, J. Helgesson, P.E. Lindelof, M. Manninen, *Phys. Rev. B* **58**(12), 8111 (1998)
56. H. Hakkinen, U. Landman, *Phys. Rev. B* **62**(4), R2287 (2000)
57. E. Janssens, H. Tanaka, S. Neukermans, R.E. Silverans, P. Lievens, *New J. Phys.* **5**, 46 (2003)
58. T. Holtz, P. Lievens, T. Veszpremi, M.T. Nguyen, *J. Phys. Chem. C* **113**(49), 21016 (2009)
59. P. Saha, A.B. Rahane, V. Kumar, N. Sukumar, *Phys. Scr.* **91**, 053005 (2016)
60. H. Hakkinen, *Adv. Phys. X* **1**(30), 467 (2016)